N8123071

NASA Technical Memorandum 81962

TRANSONIC FLUTTER STUDY OF

A WIND-TUNNEL MODEL OF

AN ARROW-WING SUPERSONIC TRANSPORT

Charles L. Ruhlin

and

Charles R. Pratt-Barlow

APRIL 1981

NASA

TRANSONIC FLUTTER STUDY OF A WIND-TUNNEL
MODEL OF AN ARROW-WING SUPERSONIC TRANSPORT

Charles L. Ruhlin*
NASA Langley Research Center
Hampton, Virginia

and

Charles R. Pratt-Barlow**
Boeing Commercial Airplane Company
Seattle, Washington

Abstract

A 1/20-size, low-speed flutter model of the SCAT-15F complete airplane was tested in the Langley Transonic Dynamics Tunnel on cables to simulate a near free-flying condition. Only the model wing and fuselage were flexible. Flutter boundaries were measured for a nominal configuration and a configuration with wing fins removed at Mach numbers M from 0.76 to 1.2. For both configurations, the transonic dip in the wing flutter dynamic pressure q boundary was relatively small and the minimum flutter q occurred near M = 0.92. Removing the wing fins increased the flutter q about 14 percent and changed the flutter mode from symmetric to antisymmetric. Vibration and flutter analyses were made using a finite-element structural representation and subsonic kernel-function aerodynamics. For the nominal configuration, the analysis (using calculated modal data) predicted the experimental flutter q levels within 10 percent but did not predict the correct flutter mode at the higher M. For the configuration without wing fins, the analysis predicted 16 to 36 percent unconservative (higher than experimental) flutter q levels and showed extreme sensitivity to mass representation details that affected wing tip mode shapes. For high subsonic M, empennage aerodynamics had a significant effect on the predicted flutter boundaries of several symmetric modes. A follow-on research program on arrow-wing flutter is suggested.

I. Introduction

Transonic wing flutter was found to be a design problem on the United States supersonic transport.[1,2] Although considerable advanced supersonic transport AST flutter design experience was gained in that program, the transonic wind tunnel testing was limited to cantilevered models.

A current AST design concept is a blended-body, arrow-wing configuration similar to the model configuration shown in Figs. 1 and 2. Transonic flutter studies of simplified cantilevered models having a planform representative of an AST arrow-wing have indicated no unusual transonic Mach number effects on flutter and reasonably good experiment-analysis correlations using current analytical

methods.[3,4] Flutter analyses, using similar analytical methods, of conceptual AST designs have indicated mass penalties to prevent flutter that are 6 to 14 percent of the wing mass.[5-8] There is concern regarding the accuracy of these results because of the lack of experimental data on models that include wing-root freedoms for validation of analyses. Another reason for concern is that AST configurations characteristically have a large number of closely spaced low-frequency, plate-like vibration modes that couple readily into a complicated flutter mode. The structural complexity of AST aircraft makes it difficult to reliably predict by existing procedures the modal characteristics which are a vital ingredient in the flutter analysis. The free-root wing flutter analyses and related wind-tunnel testing described herein add some insight to the sensitivity of AST wings to changes in the technique of mathematically modeling the structure, and are presented as a part of the continuing effort to improve the capability to predict transonic flutter characteristics.

In 1968, the Boeing Company tested and analyzed a 1/20-size, low-speed flutter model of the SCAT-15F arrow-wing design. This model was later made available by the Federal Aviation Administration for testing by the National Aeronautics and Space Administration (NASA). The SCAT-15F configuration is similar to current AST arrow-wing designs. A finite-element mathematical representation of this model, formulated in the earlier study, was also made available.

A joint NASA-Boeing program was initiated to measure the transonic flutter characteristics of this SCAT-15F model and to examine how well current analytical methods can predict the experimental results. The flutter tests were conducted in Freon in the Langley Transonic Dynamics Tunnel with the model mounted on a cable system that provided a near free-flying condition. Two configurations were tested, a nominal configuration and one having the vertical fins on the wing removed. The former was tested to provide a flutter data base, the latter because the wing-fin removal was predicted to have a significant favorable effect on flutter. For comparison with experiments, vibration and flutter analyses were made using a finite-element structural representation of the model and subsonic lifting-surface (kernel function) theory.

To prepare for these transonic tests, the model was refurbished, equipped with new, flow-through engine nacelles, structurally modified for mounting on the cables, and several ground vibration surveys were made. Analytical efforts included a low-speed flutter analysis to identify model parameter variations for the transonic tests, mathematical model

---

improvements, calculation of transonic stability derivatives, and calculations to verify stability of the model on the cable-mount system design.

Reported herein are the experimental and analytical results of this study, including highlights of the test preparation efforts. Also, a follow-on experimental research program on the flutter of arrow-wing AST aircraft is suggested. Additional results and details of this study are contained in two annual NASA contractor reports on supersonic cruise vehicle research[9,10] and in a follow-on report of this series which will be published later in 1981.

II. Experiments

Model

General. The 1/20-size, dynamically and elastically scaled model of the complete SCAT-15F airplane is shown in Figs. 1 and 2. Model scaling ratios and dimensionless similarity ratios for low-speed and transonic test conditions are presented in Table I. The model was tested transonically in Freon to achieve a mass density ratio more representative of the full-scale vehicle. Note that the reduced-velocity, mass-density, and Froude number ratios are no longer unity for a transonic test, since the model was designed for low-speed tests. Although these deviations from ideal model scaling were not significant for the present research, they are important in the interpretation of model flutter data to full-scale airplane values. It should also be noted that roughly half the model mass was supported on a lift cable in the transonic tests, which together with the Froude number ratio shown in Table I, resulted in the model flying at the wrong angle of attack.

The model was designed to scale the airplane in an operating empty weight condition. The wing stiffness level of the model represented 75 percent of the nominal airplane stiffness. The wing had a 3-percent-thick airfoil section. The horizontal tail, vertical tail, wing fins, and engine nacelle beams were constructed as comparatively rigid structures. The model also had a stiff ventral fin that was added during the low-speed tests to improve the directional stability. For the transonic tests, the model was refurbished, equipped for testing on the cable-mount system, and the original solid engine nacelles were replaced with dynamically similar flow-through nacelles of the same external shape.

Some model mass properties are listed in Table II. To attach the model to the cable-mount system, additional structure and mass ballast were required in the fuselage that amounted to about 40 percent of the airplane payload mass. The horizontal tail was all-movable in pitch and was remotely operated via an electric drive motor in the aft fuselage for longitudinal trim. No other control surfaces were modeled

Construction. The wing was scaled to represent the chordwise and spanwise stiffness distribution of the honeycomb-sandwich structure of the airplane. The load carrying members and most skin sections of the model wing were made of a fiberglass-sandwich-type structure using a balsa wood or plastic foam core. The main wing box was constructed of an internal lattice of shear ribs and spars which was bonded to the sandwich skin covers. In the wing trailing-edge flap area, thin mylar was used in place of the sandwich skins. Wing stiffness distribution was achieved by varying the number of fiberglass layers in the wing spar and skin elements. In the wing apex area, the wing and fuselage were made as a single continuous surface.

The stiffness of the fuselage section adjoining the wing was incorporated in the wing carry-through structural box. The stiffnesses of the remaining forward and aft sections of the fuselage were provided by two aluminum-alloy spars cantilevered from the wing box. Ballasted shell sections, consisting of a balsa wood frame and thin fiberglass covers, were attached to the fuselage spars and wing box to form the fuselage external contours and provide the scaled mass properties.

Construction of the tail, ventral-fin and wing-fin surfaces was similar to that of the main wing structure. Each flow-through nacelle was made of an aluminum tube with balsa wood fairings to form the external shape and with lead weights to provide proper ballast. Each nacelle was attached by a rigid beam to the wing rear spar and the transverse auxiliary nacelle spar. The model was equipped with pulleys and brackets for attaching the cables of the mount system.

Instrumentation. The model was equipped with strain gages to measure the chordwise and spanwise bending at five different wing stations and the vertical and lateral bending at three fuselage stations. A servo-accelerometer was mounted in the fuselage to measure the static pitch angle. The model instrumentation leads were routed along the four safety (snubber) cables out of the wind-tunnel test section.

Vibration Characteristics

Ground vibration surveys to measure the natural frequencies, damping ratios, and node lines of various model configurations were made at different stages of this study. Vibration mode shapes, however, were not measured for the tested configurations. Presented in Fig. 3 are the measured frequencies, structural damping ratios g, and node lines associated with the first seven or eight natural vibration modes of the two tested configurations. Included in this figure are calculated modal data for comparison later in this report. The removal of the wing fins had little effect on the basic nodal patterns, but caused an increase in frequency of the two or three lowest frequency modes and a shift in the order of the two lowest frequency antisymmetric modes.

The experimental data were measured immediately prior to the transonic tests in a calibration lab with the model mounted on a near duplicate of the tunnel cable system. In these vibration surveys, because the constraints imposed on the model by the cables vary somewhat with cable geometry, the model was centered on the cable system by a low-frequency spring in a manner similar to that shown in Fig. 2. The vibration modal data were measured with a rear-cable tension of 845 N (190 lbf), the nominal wind-tunnel test value. No attempt was

made to simulate model drag forces that would increase the forward cable tension during a test. A comparison of modal data measured with the rear-cable tension reduced by one-half indicated that, overall, the tension change had only a minor effect on the vibration modes.

For most of the ground vibration surveys an electro-magnetic shaker with a maximum output force of 4 N (1 lbf) was attached to the fuselage near the model center of gravity and oriented to provide either a vertical or lateral excitation force. For some modes, the shaker was relocated to another fuselage station or two shakers were located on the wing apex just outboard of the fuselage. The fundamental natural frequencies of the individual tail surfaces, wing fins, and engine nacelles, measured in as near a cantilevered condition as possible, were above 32 Hz.

The rigid-body frequencies and damping ratios g of the model on the cable-mount system with the low frequency spring and with the spring effect removed mathematically are:

	Plunge	Pitch	Roll	Yaw	Side
With spring, Hz	1.06˙	1.18	1.31	1.15	0.89
No spring, Hz	0.60	1.16	1.17	1.15	0.83
g(average) =	0.15	0.02	0.04	0.04	0.20

Flutter analysis of the nominal configuration at $M = 0.90$ confirmed that there was no appreciable effect from including a spring simulation of the cables to approximate the measured rigid-body frequencies. However, a simulation of the spring effects of the cables was included in the analyses for completeness.

Transonic Tests and Procedures

Wind Tunnel. The transonic tests were conducted in Freon*-12 in the Langley Transonic Dynamics Tunnel. This tunnel has a 4.88-m (16-ft) square, slotted test section with cropped corners. It is a continuous-flow tunnel that can be operated at Mach numbers up to 1.2 in air or Freon over a wide range of test-medium densities. Mach number and dynamic pressure can be varied simultaneously or independently. The tunnel is equipped with four, quick-opening bypass valves which, when actuated, can rapidly reduce the Mach number and dynamic pressure in the test section.

Mount System. The model was tested by the Boeing Company in 1968 in the Convair low-speed tunnel at San Diego, California, on a rod and trunnion mount system that provided a free-flight simulation. For the transonic tests, the model was modified for testing on a cable-mount system (see Figs. 1 and 2) that also provided a near free-flying condition. On this system, the model fuselage was supported on the tunnel centerline by a forward cable in the vertical plane of the tunnel and a rear cable in the horizontal plane. The ends

*Freon: Registered trademark of E. I. DuPont de Nemours and Co., Inc.

of the forward cable were pinned to the fuselage, forming a closed loop that ran forward from the model through the ceiling, around the test section, and back through the floor to the model. The rear cable was fastened at one end to the tunnel side-wall, ran forward through pulleys in the model, and then rearward to the opposite sidewall. The forward cable was oriented at about 48° to the horizontal plane, the rear cable at about 22° to the vertical plane. The rear cable loop included a spring that could be remotely controlled to vary the tension in the cable system. Four safety snubber cables were attached to the fuselage near the model center of gravity. The snubber cables were routed through the sidewall slots to a remotely-controlled damper-piston actuator system. In Fig. 2(b), a technician is shown holding a snubber cable. When engaged, the snubber cables restrained the model in its centerline position. A lift cable system supported the model near its center of gravity (see Fig. 2(a)), allowing free translation while continuously supporting the desired proportion of the model mass.

Test Procedure. Each tunnel test run was conducted by holding a constant total pressure and increasing Mach number M (with an accompanying increase in dynamic pressure q) until either flutter occurred or the tunnel M limit was reached. Generally, the initial run on a model configuration was made at a low total pressure and for each successive run the total pressure was stepped-up until a flutter boundary had been defined. When flutter was encountered, the bypass valves were manually actuated to reduce rapidly the M and q in the test section, thus causing flutter to subside quickly.

During the tests, the model was visually monitored by observers in the tunnel control room. Selected dynamic responses and static loads of the model, as measured by signals from the strain-gages, were recorded and visually monitored on direct read-out, oscillograph recorders (strip-charts), and recorded on analog magnetic tape. A real-time analyzer was used to provide a frequency spectrum of the wing-root motion during the test. High-speed movies were taken at flutter onset or to record model flight behavior. Continuous visual records of the model flight were made on video tape. Tunnel-flow conditions were tabulated at selected points and at flutter by an automated, digital data system.

After the first test run, the rear cable attachments were lowered about 30 cm (1 ft) to permit the model to be flown normally in a trimmed condition in the center of the test section by the pilot via the all-movable horizontal tail. The lift-cable tension was held at roughly half the model weight 133 N (30 lbf) throughout the test. The tension in the rear flying cable was roughly 845 N (190 lbf) and the front cable tension varied between 530 to 1290 N (120 to 290 lbf), depending on the model drag.

Test Results

The transonic test results are tabulated in Table III and presented as boundaries of flutter dynamic pressure q against Mach number M in Fig. 4. A transonic flutter boundary had been established for the nominal configuration and a partial boundary for the configuration with wing fins removed when the model loss ended the test.

The flutter point from the low-speed test of a near-nominal configuration is included in Fig. 4. This low-speed flutter point was obtained in air and was adjusted to apply to Freon on the basis of flutter analyses for the model in air and Freon.

The model was lost due to a static structural failure that occurred near $M = 0.99$. Although normally the model was easily trimmed and flew quite well, the configuration without wing fins had a tendency to rise or fall somewhat randomly at Mach numbers from about 0.97 to 1.03. Consequently, it was necessary to frequently retrim the model with the horizontal tail to keep it within about 15 cm (6 in.) of the centerline. Prior to the failure, the model rose in the tunnel, was retrimmed, then slowly dropped to the limit of the lift cable, and finally pitched nose down rather quickly. At this time, the fuselage forebody broke off under the down load causing the wing to pitch up and disintegrate. The model was not lost due to flutter but rather to a flight trim control problem.

For both configurations tested, the flutter mode appeared to involve motion primarily in the wing-tip region. For example, during symmetric flutter of the nominal-configuration, the wing fin appeared to follow the wing motion with a node line running spanwise from slightly ahead of the wing-fin leading edge to the wing trailing-edge break (at FS 395). The nominal configuration also had a symmetric 11 Hz mode that was very lowly damped and appeared to be on the verge of flutter as indicated by the frequency spectra shown in Fig. 5.

It can be seen (Fig. 4) that the transonic flutter boundary for the nominal configuration is rather flat, and, based on the adjusted low-speed flutter point, remains flat in the low subsonic range. Removing the wing fins did increase the flutter q but not as much as expected from the low-speed parametric analytical study, and changed the flutter mode from a 16-17 Hz symmetric to a 19-20 Hz antisymmetric mode. The antisymmetric flutter boundary of the configuration without wing fins had a more usual transonic dip shape but this amounted to less than a 10-percent decrease from the flutter q at $M = 0.81$. For both configurations, the minimum flutter q occurred near $M = 0.92$.

III. Analytical Methods

Mathematical Representation of Model

The original finite-element representation simulated only the basic wing and fuselage structure for symmetric analyses. In the present study, this mathematical model was adapted for use in a new integrated structural analysis and design program ATLAS,[11] expanded to include a representation of all the model surfaces (e.g., tail surfaces and ventral fin), and modified to allow antisymmetric analysis.

The finite-element representation of the model, shown in Fig. 6, consists of about 560 structural nodes and 1500 structural elements. A gross stiffness matrix of about 2200 degrees of freedom was reduced to about 350 freedoms to perform the modal analyses. Symmetric two-node spars with appropriate web and flange areas were used to represent each of the spars and ribs in the model. Isotropic

plates of appropriate gage were used to represent the model skin. The stiffness values used for the fiberglass-sandwich structures were based on test specimen measurements during model construction.

A check on the finite-element modeling of the basic wing was made shortly after construction by comparing calculated structural influence coefficients with measured values; the agreement was considered good. Test values were obtained by cycling the loading to eliminate hysteresis and creep effects. Unfortunately, the wing tip torsional deflections were not measured. For the present analysis, the fictitious beam elements used in the original flat-wing representation to account for wing-crease stiffening effects were removed and the actual crease geometry incorporated.

Vibration Analysis and Unsteady Aerodynamics

The model mass distribution data (calculated during model construction) was reduced to a lumped-mass system at the vibration analysis nodes. When the cable-mount system was simulated in the analysis by spring representations at the cable attachment points, the fore-and-aft translation was locked out at the fuselage centerline.

The flutter analysis was based on subsonic lifting-surface (kernel function) unsteady aerodynamics theory. Planform discontinuities were smoothed to minimize numerical integration errors. The aerodynamic collocation points were distributed over the half-span model, and centerline boundary conditions applied to generate the symmetric and antisymmetric unsteady aerodynamic forces. The location and number of downwash chords and the number of points per chord were varied until near-converged values were obtained for the aerodynamic terms. Nine downwash chords were used on the wing with nine points per chord and four downwash chords each on the wing fin, the horizontal tail and the vertical tail, with five points per chord. The calculated modal displacements at the structural grid points were interpolated to the displacements and slopes at the points required by the aerodynamic theory using a plate surface interpolation method.

Flutter Analysis

Flutter analyses were made for the Mach numbers corresponding to the low-speed and transonic test points, with the exceptions that the highest Mach number used was 0.935 and additional subsonic Mach numbers were included to help define the transonic flutter boundaries. At each value of M, a flutter frequency f and dynamic pressure q of the flutter modes were calculated for a velocity that exactly matched that in the wind tunnel at that M. Typically, V-g data were generated at one M for each of several density values, and the resulting flutter data cross-plotted to obtain the matched point. A total of twelve modes were used in each analysis and included the first ten calculated symmetric vibration modes or the first nine calculated antisymmetric vibration modes and the rigid-body modes on the cable support. The measured damping ratios for these modes were used. In some instances, a p-k flutter solution technique was used to clarify the subcritical branching behavior of the aeroelastic modes.

4

IV. Pre-Test Analyses

Flutter Parameter Analysis

Flutter analyses were made early in the present study to identify model flutter parameters that could be varied most usefully in the transonic tests. These analyses were restricted to the symmetric case, $M = 0.21$ in sea-level air, and full-payload, nominal configuration. (The full payload condition would amount to an increase in distributed fuselage weight of about 2.27 kg (5 lbm) over the transonic-test nominal configuration.) The wing-fin aerodynamic forces were found to have negligible effect on the flutter and, therefore, were normally not included in the analysis when the effects of varying other parameters were determined.

The results for the parameter variations that affect the low-speed flutter significantly are shown in Fig. 7. Generally, these parameters were found to be important in the flutter of AST-type aircraft in earlier studies.[1,5] The following parameter variations were also analyzed but had less than a 10-percent effect on the flutter q:

(1) Including wing-fin air forces.

(2) Removing horizontal tail air forces.

(3-5) Removing nacelles: (3) outboard, (4) inboard, and (5) all.

(6-7) Varying nacelle weight (rigid attachment): (6) 33 percent heavier, and (7) 33 percent lighter.

(8-9) Varying nacelle position (rigid attachment): (8) 6.35 cm (2.5 in.) forward and (9) 6.35 cm aft.

Based on these results, the configuration with wing fins removed was selected for transonic testing in addition to the nominal configuration. A second wind-tunnel entry was planned to study the effect of stiffening the wing-tip region. On the model, altering the engine nacelle beams was not a practical consideration because the beams were bonded internally to the wing spar structure.

Low-Speed Test Correlation

Experimental and analytical correlations with the 1968 low-speed test data were made to verify the model integrity after removal from storage and to check for errors in the finite-element model after it had been modified for the present study. The frequencies and node lines of the first eight symmetric vibration modes were both measured and calculated for the nominal low-speed test configuration. Overall, these data agreed well with each other and with the 1968 test data. The flutter characteristics for this configuration were then calculated using the calculated modal data for these eight symmetric modes without structural damping. The resulting flutter results were essentially the same as that calculated in 1968. It should be noted that in the 1968 low-speed study, the calculated flutter speeds were about 20 percent lower than the experimental values, and the correct critical flutter mode was obtained only when measured structural damping values were included in the analyses. Also in that study, using the higher measured

frequencies for the vibration modes improved the agreement in flutter speed in contrast to the present analytical results that are discussed later. In the present study, the mathematical representation was improved by redistributing the lumped-masses in the wing-tip region as shown in Fig. 8, and the vibration and flutter analysis was redone. This analysis, which also used measured structural damping values, not only predicted the correct flutter mode but also a flutter speed that was very close to the experimental value. The new calculated vibration mode frequencies also matched experiment better with nodal patterns similar to those shown for the transonic-test nominal configuration in Fig. 3.

Thus, it was concluded that the wind-tunnel model was physically sound and that the revised, modified-tip mathematical modeling was quite good. These results point out the importance of the wing-tip region in the flutter of arrow-wing configurations and the need to accurately represent the wing tip in both the analytical and physical models.

Cable-Mount Stability Analyses

In the low-speed tunnel tests, the model was unstable in pitch on the basic rod and trunnion mount system but was stabilized by a cable and air-spring arrangement that provided a pitch couple about the model center of gravity and additional damping in pitch. Extensive cable-mount dynamic stability analyses were made at the expected test conditions for the two transonic-test model configurations. Stability derivatives for these analyses were generated by the FLEXSTAB[12] program for both the rigid and flexible model cases using Woodward first order unsteady aerodynamic terms for subsonic Mach numbers and for $M = 1.2$.

The calculated derivatives were employed in the dynamic stability analysis program developed for models on the Langley cable-mount system. The analyses covered the same Mach number range as the calculated derivatives, several dynamic pressure values, and a wide range of cable-system variables. Based on these analyses, the cable-mount system previously described was designed. To improve the lateral stability, a lift cable was included to support about one-half the model weight during the tests.

The stability analyses indicated that, in general, the stability (damping) of the model on the cable mount (1) increased with increasing q, and (2) decreased with increasing M. Removing the wing fins had only a slight and usually stabilizing effect. A comparison of the stability results obtained using the rigid and flexible data indicated that the flexible model was slightly more stable. No specific wind-tunnel tests were made to verify these stability results. During most of the test the model was quite stable and easily trimmed.

V. Transonic Test-Analysis Correlations

Mathematical Model Refinements

Following the transonic tests, the model mass properties and cable-mount spring simulations were updated in the mathematical model to match the test configurations. Because doubt had been cast

on the fidelity of the original wing lumped-mass system by the need to refine the wing tip representation for good low-speed flutter test-analysis correlation, the mass data calculated during model construction were set up as a combination of distributed and localized masses using ATLAS mass elements and concentrated mass data. Different engineering approximations for lumping the wing mass at the refined set of retained nodes created seemingly minor perturbations in the vibration mode frequencies and mode shapes. However, the different mass representations created aerodynamic variations, apparently via subtle node line shifts and mode shape changes, that were responsible for a disturbingly large band of uncertainty (scatter) in the predicted flutter q for several of the analytical flutter modes as discussed in the following sections.

Vibration Characteristics

The vibration characteristics of the two test configurations were calculated using the lumped-mass system considered to best represent the actual wing mass data, and the resulting frequencies and node lines of the first seven vibration modes are included in Fig. 3. It can be seen that the nodal pattern of each calculated mode is in basic agreement with the nodal pattern of the corresponding measured mode. Although the test-analysis frequency comparison for some modes is not particularly good, the overall correlation in the frequencies and nodal patterns is considered to be satisfactory. Some pictorial sketches of the pertinent mode shapes are shown in Fig. 9. Because the mode shapes for the two configurations are roughly similar, only the symmetric mode shapes for the nominal configuration and the antisymmetric mode shapes for the configuration without wing fins are presented. For symmetric flutter of the nominal configuration, the corresponding analytical mode had as its aerodynamic drivers (established from an energy balance calculation) predominantly mode 5 and, to a lesser degree, modes 6 and 7 (Fig. 9(a)). For antisymmetric flutter of the configuration without wing fins, the aerodynamic drivers were predominantly mode 5, and, to a much lesser degree, modes 6, 7, and 8 (Fig. 9(b)).

Flutter Characteristics

Symmetric and antisymmetric flutter analyses of the two test configurations were made using the calculated mode shapes and frequencies but measured damping values. An early flutter analysis indicated that using the measured frequencies in place of calculated frequencies produced no significant improvement in flutter correlation; therefore, the calculated frequencies were used in all of the transonic correlation analyses.

The analytical flutter solutions are compared with the experimental boundaries in Figs. 10 and 11. The effects of empennage aerodynamics on the analytical flutter modes are isolated by comparison of the results in the (a) and (b) part of each figure. These analyses were made using the calculated modal data previously presented (Figs. 3 and 9) for the lumped-mass system considered to best represent the actual wing mass. In efforts to improve the test-analysis correlations, the effects of several variations in the wing tip lumped-mass representation were examined and the

results are presented in the (c) part of each figure. Any one of these different lumped-mass representations has been considered reasonable in the past for flutter analysis because of the degree of refinement in each representation.

Nominal Configuration. The flutter analyses for the nominal configuration predicted two symmetric flutter modes to be critical, whereas only one flutter mode, corresponding to the higher frequency 14-16 Hz analytical mode, was obtained in the test. However, it should be recalled from the transonic test observations that a lower frequency, 11 Hz mode was on the verge of flutter. Thus, the analyses did identify correctly the potential flutter modes. The effects of removing the empennage aerodynamics from the analyses were to reduce slightly the flutter q levels of both modes and to alter the M trends somewhat (Figs. 10(a) and 10(b)). A review of the transonic-test response records indicated no appreciable aft-fuselage response in the higher frequency, 16-17Hz symmetric flutter mode. Therefore, the analytical results most consistent with the model test behavior are those in which the empennage aerodynamics were excluded for the 14-16 Hz analytical mode.

Based on the above considerations, the most test-consistent boundaries for the two analytical modes are presented in Fig. 10(c). Variations in the wing-tip lumped-mass representation produced about a 15 percent scatter in the predicted flutter q for these modes as indicated by the shaded portions around each analytical boundary. In general, these variations raised the predicted flutter q levels for both modes. It can be seen that the analysis did predict the correct flutter mode at M < 0.78, but did not at the higher Mach numbers. The test flutter q levels were predicted reasonably well. Overall, the test-analysis correlation was considered good.

Configuration with Wing Fins Removed. For this configuration, four different modes were predicted as potential flutter modes (Fig. 11(a)). The empennage aerodynamics had a significant effect on the 5-6 Hz and 12-13 Hz symmetric modes. The empennage added aerodynamic damping in the 5-6 Hz mode to raise the flutter q sufficiently high for this mode to be of no concern as a flutter mode and it was, therefore, excluded from Fig. 11(c). The original low-speed analysis, which did not include the empennage aerodynamics, indicated this 5-6 Hz symmetric mode to be a potential flutter mode. However, empennage aerodynamics reduced the flutter q on the 12-13 Hz mode to a level of concern. As for the nominal configuration, the empennage aerodynamics for the 16-17 Hz symmetric mode were neglected in the data presented in Fig. 11(c).

Although the test flutter point at M = 0.81 involved mostly antisymmetric motion, it was not well defined "hard" flutter and considerable symmetric motion was noted in the response records indicating the proximity of a lowly damped symmetric mode. Thus, the analytical prediction of the presence of symmetric flutter modes is not unrealistic.

The flutter boundaries considered as consistent with the test results are presented in Fig. 11(c).

6

For these modes, variations in the wing tip lumped-mass representations produced an alarmingly large scatter in the predicted flutter q. The scatter as a percentage change in flutter q from the sharp flutter boundary for each mode shown in Fig. 11(c) is indicated below:

Mode	From boundary, percent	
	Below	Above
18-20 Hz antisymmetric	15	21
16-17 Hz symmetric	7	52
12-13 Hz symmetric	13	2

This scatter obviously clouds the test-analysis correlation. As a general observation, the analysis tended to predict 16 to 36 percent unconservative (higher than experimental) flutter q levels, and did identify as potentially critical, several modes which included the test flutter mode. The results point out the need for more analytical and experimental studies on arrow-wing configurations to better understand the effects of these different mass representations.

VI. Summary of Results

An analytical and wind-tunnel study of a 1/20-size, complete airplane model of an arrow-wing supersonic transport (SCAT-15F) has been made. Flutter boundaries for a nominal configuration and for a configuration without wing fins were measured at Mach numbers M from 0.76 to 1.2 with the model mounted on cables to simulate a near free-flying condition. Flutter analyses using calculated modal data and subsonic lifting-surface (kernel function) aerodynamics were made for correlation with experiment. The results are summarized as follows:

1. For the two tested configurations, the transonic dip in the flutter dynamic pressure q boundary was relatively small with less than a 10-percent decrease in flutter q for the configuration without wing fins, which had the more severe dip. The minimum flutter q occurred experimentally near M = 0.92.

2. Removing the wing fins increased the experimental flutter q about 14 percent from M = 0.80 to 0.92 and caused a change in the flutter mode from symmetric to antisymmetric.

3. For the nominal configuration, the analyses correlated with the previously obtained low-speed test results very well and the experimental transonic flutter q levels within 10 percent, but did not predict the correct flutter mode at the higher transonic Mach numbers.

4. For the configuration without wing fins, the analyses predicted 16 to 36 percent unconservative (higher than experimental) flutter q levels, but the correlation was clouded by extreme sensitivity of the flutter modes to wing tip lumped-mass representations. Apparently the different mass distributions caused aerodynamic variations, via subtle mode shape changes and node line shifts, that resulted in a large band of uncertainty in the predicted flutter q for several of the analytical

flutter modes (for example, 42-percent scatter for one flutter mode).

5. The empennage aerodynamics had a significant effect on several of the predicted symmetric flutter modes.

VII. Suggested Follow-On Research

The present study leaves uncertainty regarding the adequacy of state-of-the-art analytical methods in predicting the transonic flutter characteristics of arrow-wing AST aircraft configurations. Although the present analysis is judged to have predicted the flutter characteristics of the nominal configuration acceptably well, of particular concern are the unconservative flutter q predictions with wing fins removed and the extreme sensitivity to different lumped-mass idealizations. Specific causes for these discrepancies have not been identified, in part because the lack of measured vibration mode shapes did not admit isolation of structural dynamics errors. However, the present analyses did focus attention on problem areas and raised these unanswered questions: (1) Is the flutter, in fact, as sensitive to the wing tip modal characteristics as analyses indicated? (2) If so, can a flutter-clearance-type, scaled model be built to simulate the wing tip structure accurately enough to reflect this sensitivity? (3) Why does the analysis predict the flutter characteristics for the nominal configuration so much better than it does for the configuration without wing fins?

Other potentially significant parameter variations for arrow-wing flutter that have yet to be examined experimentally are local angle of attack effects, wing tip skin stiffness, and engine nacelle beam flexibility. While some of these parameters can be successfully explored with cantilevered wing models, a complete model test is required because of question (3) above and the importance of empennage aerodynamics for certain flutter modes. To address these problems, the following research program that combines experiments and analyses is suggested.

An airplane design would be selected that would provide data directly applicable to the current AST arrow-wing designs. A master mathematical simulation of this design would be formulated. Two types of models would be designed and constructed--a series of low-cost simplified plate models and an expensive, replica-type flutter model. Both model types would be constructed for testing as cantilevered wings with eventual testing as wings on a complete flutter model. The purpose of the simplified models would be to provide early parametric trend data and to explore problem areas having greatest risk of model loss. The replica model would be used to provide more exact similitude comparisons, such as substantiating the mathematical structural representations and wing tip vibration modal characteristics, and tested to check whether the simplified model test results are as applicable as those from a more realistic scaled model. For all model test configurations, vibration mode characteristics, including mode shapes, would be very carefully measured with special attention given to the wing tip region. All tests would be correlated with analyses and causes of any discrepancies would be identified, if possible.

It is believed that the above program is a practical approach to explore these flutter problems related to arrow-wing aircraft and to provide needed validation of analyses. While there is a sizable, ongoing research effort on transonic unsteady aerodynamics, there remains a need for a rapid but accurate procedure to measure mode shapes of complex models. The correlation of flutter model test results can be used to judge relative accuracy of different transonic aerodynamic theories only when the correct mode shapes have been incorporated in the analyses. A more desirable alternative would be to determine the generalized aerodynamic forces via parameter identification from aeroelastic response measurements. It is felt that this would demand an order of magnitude improvement in quantitative accuracy and current data processing methods; it remains, however, a desirable goal.

VIII. References

[1] Turner, M. J., and Bartley, J. B., "Flutter Prevention in Design of the SST." Symposium on Dynamic Response of Structures, Stanford University, Stanford, California, June 28-29, 1971.

[2] Gregory, R. A., Ryneveld, A. D., and Imes, R. S., "A Low Speed Model Analysis and Demonstration of Active Control Systems for Rigid-Body and Flexible Mode Stability." FAA-SS-73-18, June 1974.

[3] Doggett, R. V., Jr., and Ricketts, R. H., "Some Experimental and Theoretical Flutter Characteristics of an Arrow-Wing Configuration." AIAA Paper No. 77-422, 1977.

[4] Doggett, R. V., Jr., and Ricketts, R. H., "Effects of Angle of Attack and Vertical Fin on Transonic Flutter Characteristics of an Arrow Wing." NASA TM 81914, 1980.

[5] Robinson, J. C., Yates, E. C., Jr., Turner, M. J., and Grande, D. L.: "Application of an Advanced Computerized Structural Design System to an Arrow-Wing Supersonic Cruise Aircraft." AIAA Paper No. 75-1038, August 1975.

[6] Sakata, I. F., and Davis, G. W., "Substantiating Data for Arrow-Wing Supersonic Cruise Aircraft," "Structural Design Concepts Evolution," Volume 2, NASA CR-132575-2, 1976.

[7] Sobieszczanski-Sobieski, J., Gross, David, Kurtze, William, Newsom, Jerry, Wrenn, Gregory, and Greene, William, "Supersonic Cruise Research Aircraft Structural Studies: Methods and Results." Paper No. 27 in Supersonic Cruise Research '79 - Part 2, NASA CP-2108.

[8] Gordon, C. K., and Visor, O. E., "SCAR Arrow-Wing Active Flutter Suppression System." NASA CR-145147, April 1977.

[9] Pratt-Barlow, C., Lelong, J., et al, "Advanced Concept Studies for Supersonic Vehicles," Final Contract Report, NASA CR-159028, April 1979.

[10] Pratt-Barlow, C., and Nisbet, J., et al, "Advanced Concept Studies for Supersonic Vehicles," Final Contract Report, NASA CR-159244, May 1980.

[11] Dreisbach, Rodney L., and Giles, Gary L., "The ATLAS Integrated Structural Analysis and Design Software System." "Research and Computerized Structural Analysis and Synthesis." NASA CP-2059, 1978.

[12] Tinoco, E. N., and Mercer, J. E., "FLEXSTAB--A Summary of the Functions and Capabilities of the NASA Flexible Airplane Analysis Computer System." NASA CR-2564, Dec. 1975.

Table I Model scaling ratios (Derived for airplane altitude of 4572 m (15,000 ft))

Parameter	Ratio (model/airplane)	
	Low-speed test	Transonic test
Basic scaling ratios		
Length (ℓ)	1/20	
Mass (m)	1/5033.	
Frequency (ω)	4.47	
Stiffness (EI)	4.967×10^{-7}	
Mass inertia	4.967×10^{-7}	
Dynamic pressure (ρV^2)	1/12.58	
Dimensionless similarity ratios		
Mach number	-	1.0
Reduced velocity ($V/\ell\omega$)	1.0	2.11
Mass density ($m/\rho\ell^3$)	1.0	4.47
Reynolds number	1/56.	1/84.
Froude number* ($V^2/\ell g$)	1.0	4.45

*Roughly half the model weight was supported by a lift cable during the transonic test.

Table II Model mass properties

	c.g. at FS $\frac{}{m}$	Mass $\frac{}{kg}$
Complete model	3.045	29.167
Fuselage (plus enclosed wing)	-	13.184
Exposed wing (each)	-	4.730
Nacelle (each)	3.830	1.405
Horizontal tail (each)	4.554	0.101
Vertical tail	4.511	0.209
Ventral fin	4.514	0.092
Wing fin (each)	4.168	0.199

| Inertia about center of gravity (c.g.)			
	Pitch $\frac{}{kg\text{-}m^2}$	Yaw $\frac{}{kg\text{-}m^2}$	Roll $\frac{}{kg\text{-}m^2}$
Complete model	30.581	32.191	3.336
Nacelle (each)[1]	29.53×10^{-3}	29.39×10^{-3}	1.24×10^{-3}
Wing fin (each)[2]	2.413×10^{-3}	1.929×10^{-3}	0.323×10^{-3}

[1]Each nacelle c.g. was 0.061 m (2.40 in.) below wing midchord line.

[2]Each wing fin c.g. was 0.027 m (1.04 in.) above wing midchord line.

Table III Transonic test results

Model behavior	Mach number	Dynamic pressure, kPa	Velocity, m/sec	Flutter frequecy, Hz
Nominal configuration				
No flutter	1.18	3.51	177	-
Flutter-symmetric	0.99	3.33	150	16.5
Flutter-symmetric	0.88	3.32	133	16.5
Flutter-symmetric	0.76	3.50	115	17.0
Configuration without wing fins				
No flutter	1.18	4.05	176	-
Flutter-antisymmetric	0.90	3.73	138	19.5
Flutter-antisymmetric*	0.81	4.04	123	20.9
No flutter-lost model	0.99	3.78	149	-

*Some symmetric motion evident also.
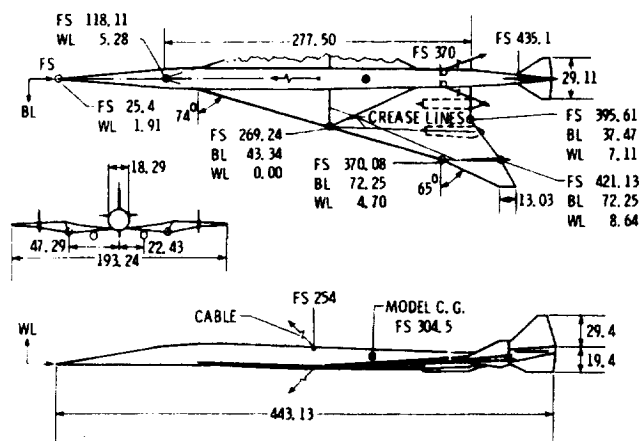
(a) THREE-VIEW SKETCHES
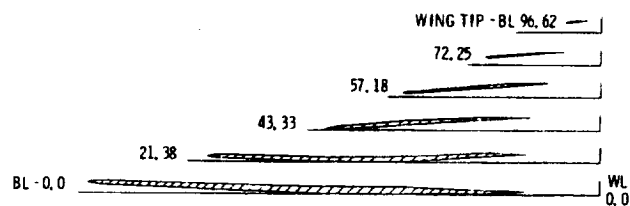
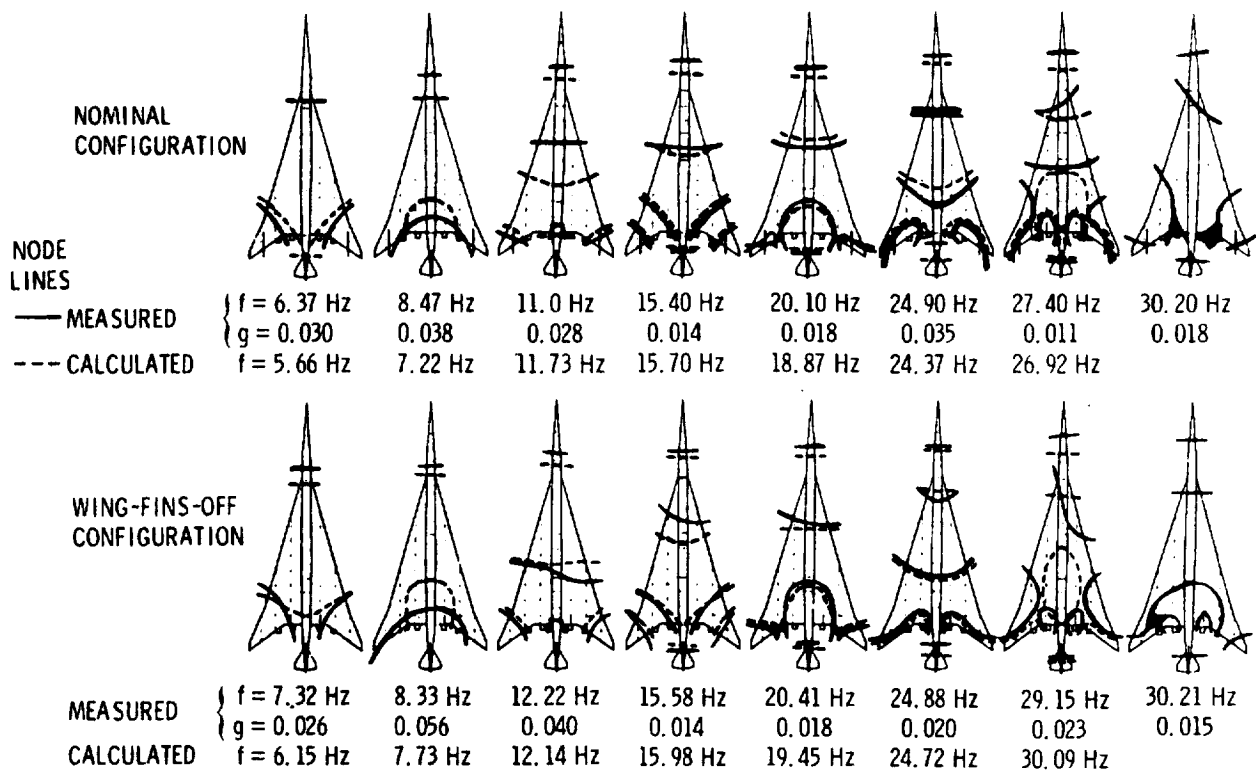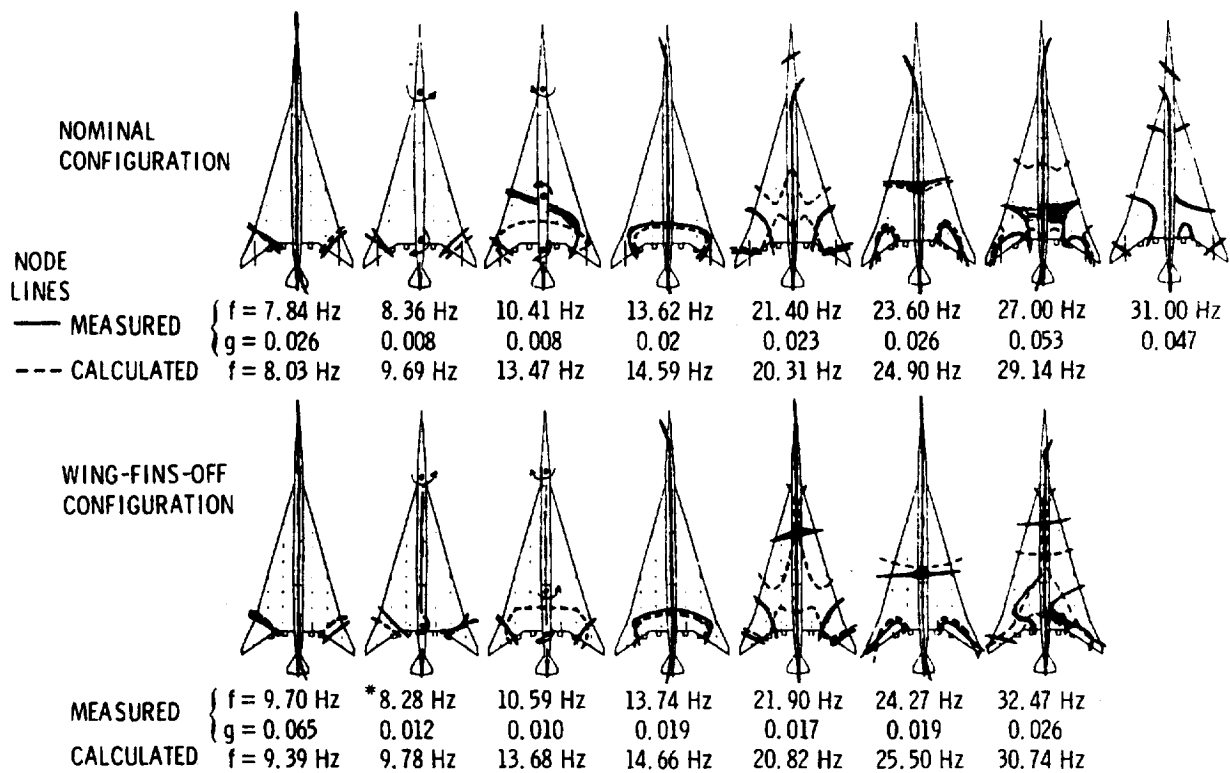(b) WING AIRFOIL SECTION AT DIFFERENT SEMISPAN (BL) STATIONS
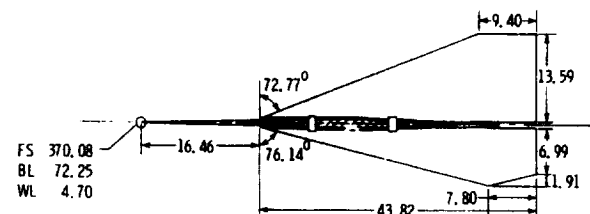
(c) WING-FIN DIMENSIONS

Figure 1.- Sketches of nominal model. Linear dimensions are in cm.

(a) Front view.

(b) Rear view.

Figure 2.- Nominal configuration in Transonic Dynamics Tunnel.

NOMINAL
CONFIGURATION

NODE
LINES
——MEASURED
- - -CALCULATED

f = 6.37 Hz	8.47 Hz	11.0 Hz	15.40 Hz	20.10 Hz	24.90 Hz	27.40 Hz	30.20 Hz
g = 0.030	0.038	0.028	0.014	0.018	0.035	0.011	0.018
f = 5.66 Hz	7.22 Hz	11.73 Hz	15.70 Hz	18.87 Hz	24.37 Hz	26.92 Hz	

WING-FINS-OFF
CONFIGURATION

MEASURED
CALCULATED

f = 7.32 Hz	8.33 Hz	12.22 Hz	15.58 Hz	20.41 Hz	24.88 Hz	29.15 Hz	30.21 Hz
g = 0.026	0.056	0.040	0.014	0.018	0.020	0.023	0.015
f = 6.15 Hz	7.73 Hz	12.14 Hz	15.98 Hz	19.45 Hz	24.72 Hz	30.09 Hz	

(a) SYMMETRIC VIBRATION MODES.

NOMINAL
CONFIGURATION

NODE
LINES
—— MEASURED
- - - CALCULATED

f = 7.84 Hz	8.36 Hz	10.41 Hz	13.62 Hz	21.40 Hz	23.60 Hz	27.00 Hz	31.00 Hz
g = 0.026	0.008	0.008	0.02	0.023	0.026	0.053	0.047
f = 8.03 Hz	9.69 Hz	13.47 Hz	14.59 Hz	20.31 Hz	24.90 Hz	29.14 Hz	

WING-FINS-OFF
CONFIGURATION

MEASURED
CALCULATED

f = 9.70 Hz	*8.28 Hz	10.59 Hz	13.74 Hz	21.90 Hz	24.27 Hz	32.47 Hz	
g = 0.065	0.012	0.010	0.019	0.017	0.019	0.026	
f = 9.39 Hz	9.78 Hz	13.68 Hz	14.66 Hz	20.82 Hz	25.50 Hz	30.74 Hz	

*FUNDAMENTAL MODE

(b) ANTISYMMETRIC VIBRATION MODES.

Figure 3.- Frequencies and node lines of natural vibration modes.

11
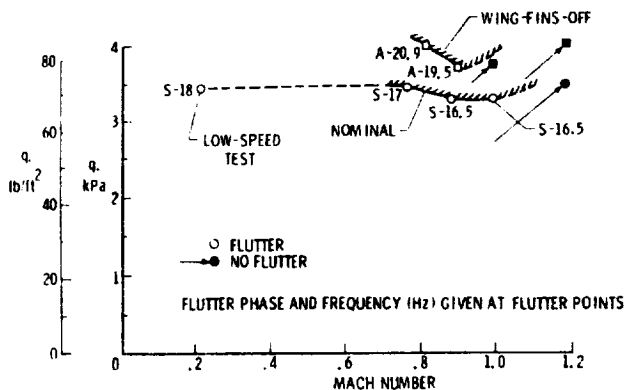
Figure 4.- Experimental flutter boundaries for nominal and wing-fins-off configurations.
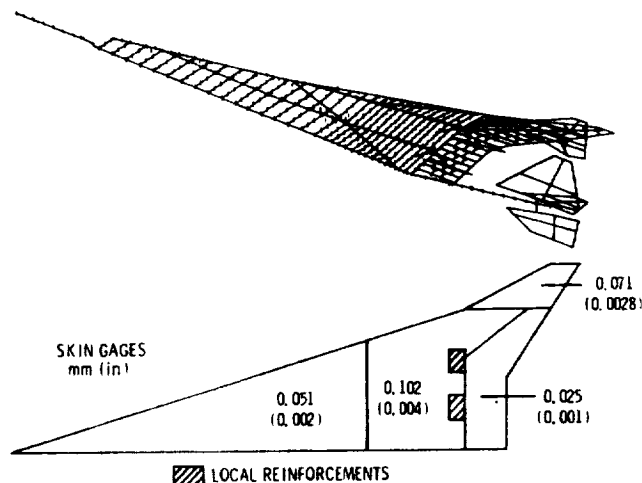

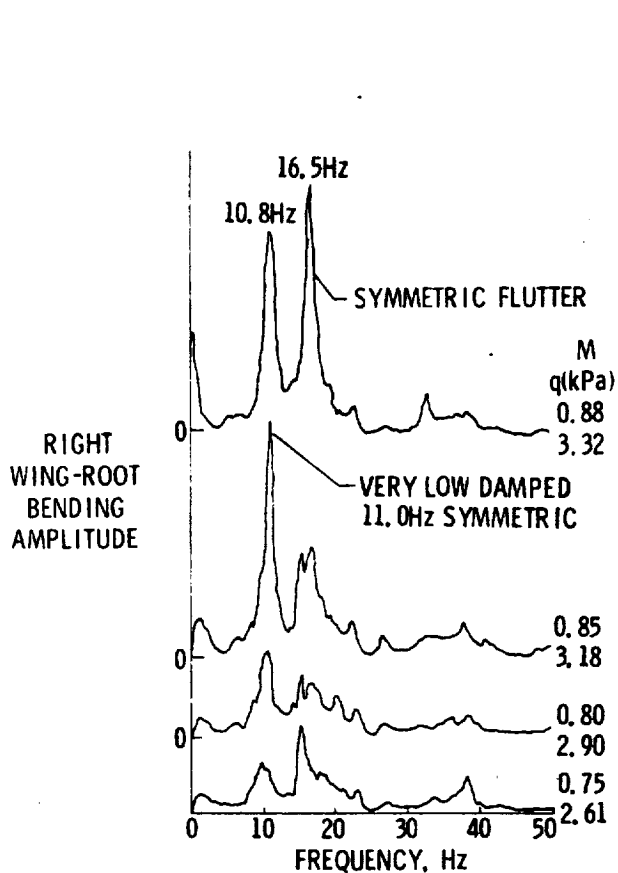Figure 6.- ATLAS finite-element structure representation.

Figure 5.- Frequency spectra of nominal configuration response to tunnel turbulence.
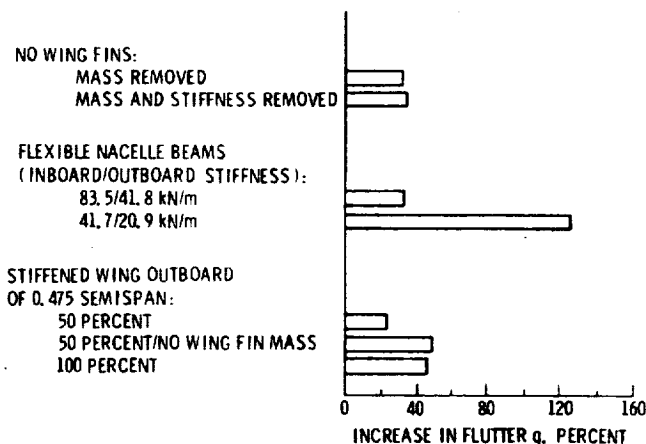

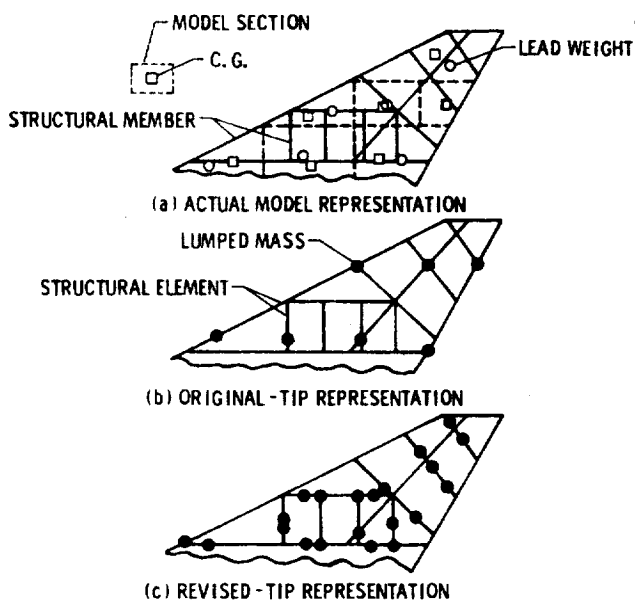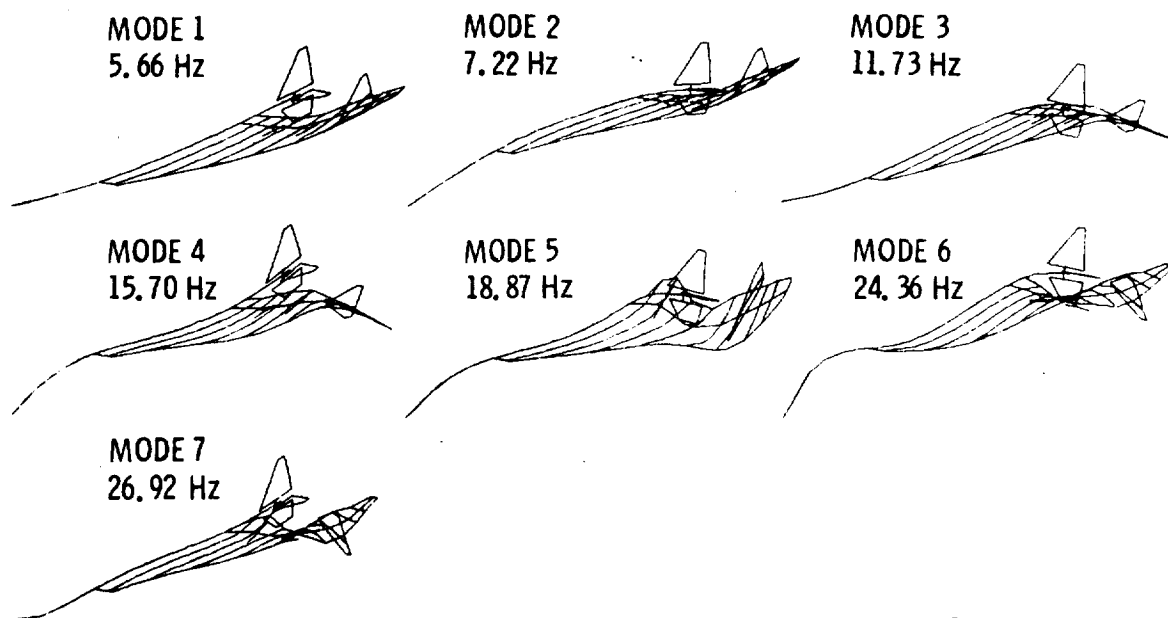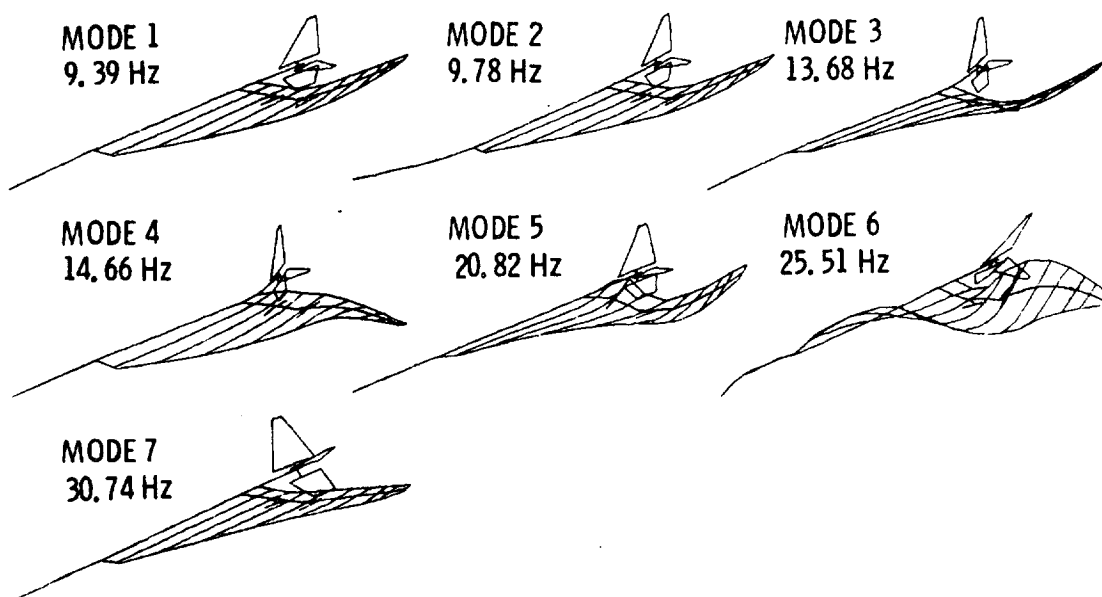Figure 7.- Results of low-speed flutter parameter analyses.

Figure 8.- Wingtip mass distribution and mathematical lumped-mass representations.

12

MODE 1
5. 66 Hz

MODE 2
7. 22 Hz

MODE 3
11. 73 Hz

MODE 4
15. 70 Hz

MODE 5
18. 87 Hz

MODE 6
24. 36 Hz

MODE 7
26. 92 Hz

(a) SYMMETRIC MODE SHAPES OF NOMINAL CONFIGURATION.

MODE 1
9. 39 Hz

MODE 2
9. 78 Hz

MODE 3
13. 68 Hz

MODE 4
14. 66 Hz

MODE 5
20. 82 Hz

MODE 6
25. 51 Hz

MODE 7
30. 74 Hz

(b) ANTISYMMETRIC MODE SHAPES OF WING-FINS-OFF CONFIGURATION.

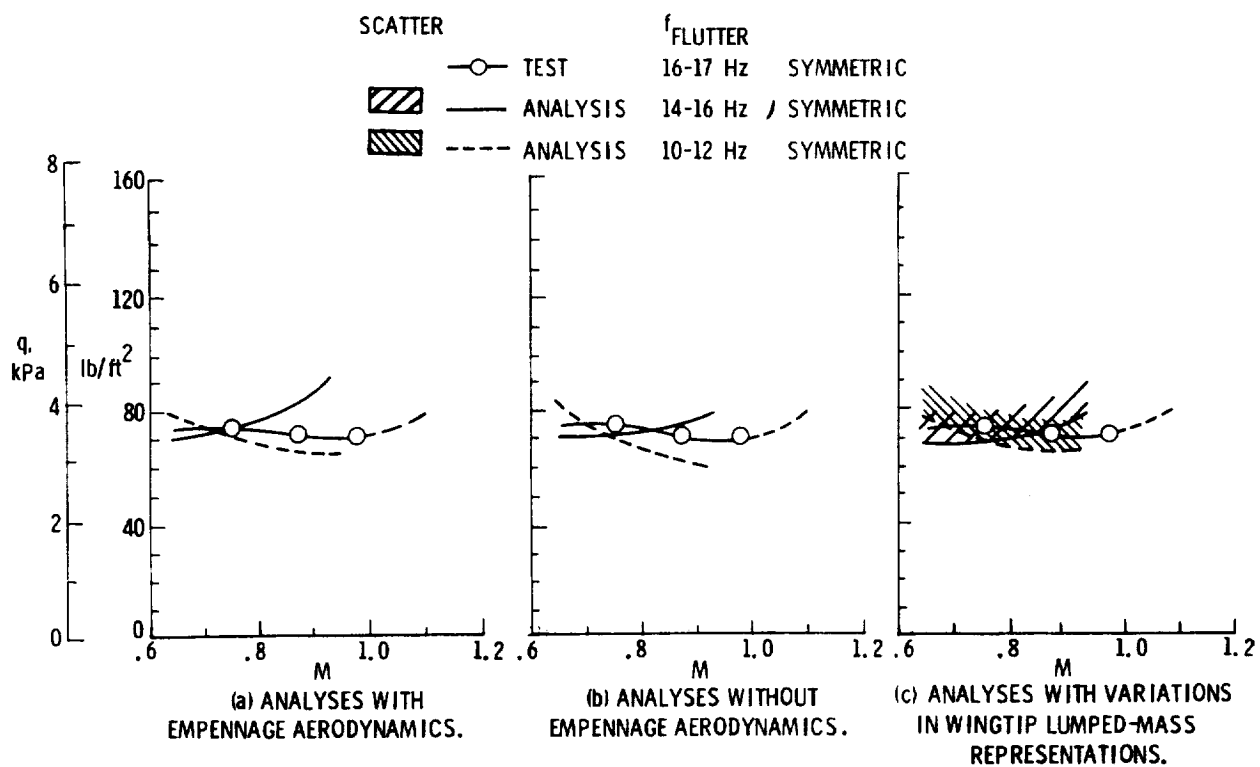Figure 9.- Pictorial sketches of pertinent vibration mode shapes.

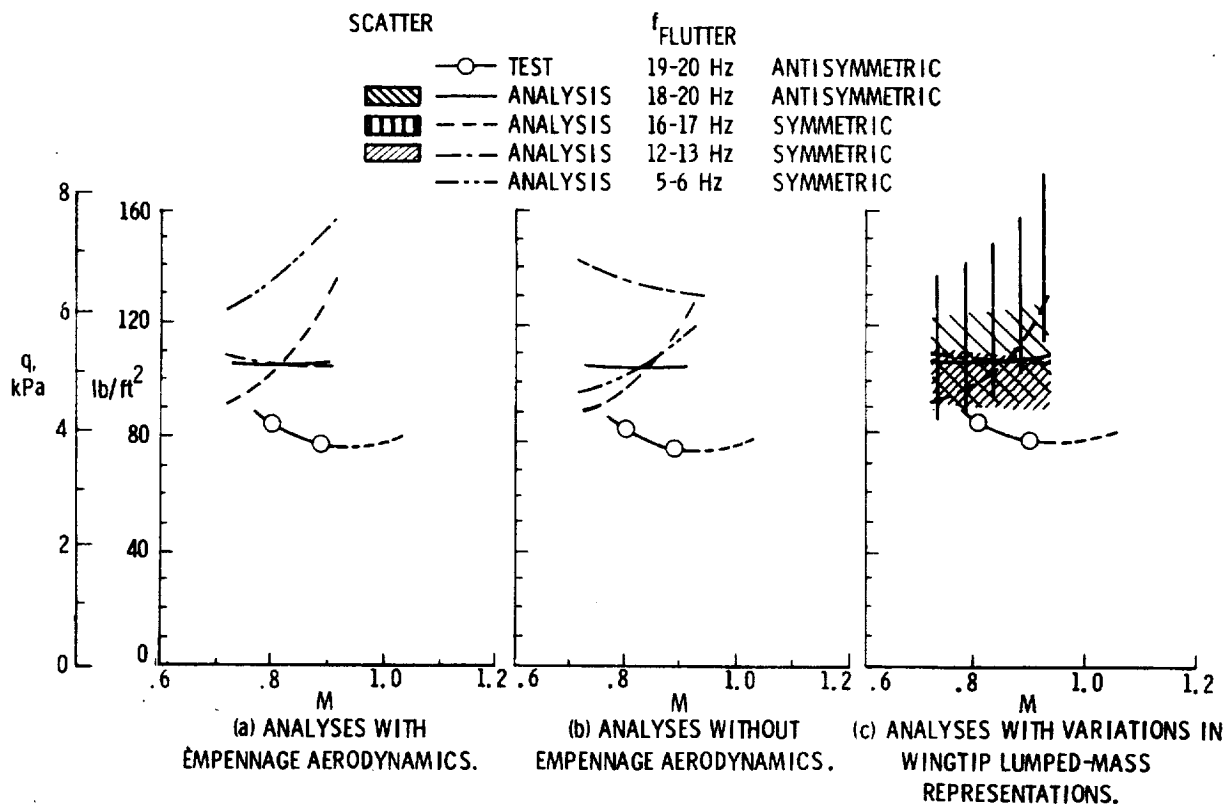Figure 10.- Calculated and measured symmetric flutter boundaries for nominal configuration.

Figure 11.- Calculated and measured flutter boundaries for wing-fins-off configuration.

14

1. Report No. NASA TM-81962	2. Government Accession No.	3. Recipient's Catalog No.
4. Title and Subtitle TRANSONIC FLUTTER STUDY OF A WIND-TUNNEL MODEL OF AN ARROW-WING SUPERSONIC TRANSPORT		5. Report Date April 1981
		6. Performing Organization Code 533-01-13-07
7. Author(s) Charles L. Ruhlin and Charles R. Pratt-Barlow*		8. Performing Organization Report No.
		10. Work Unit No.
9. Performing Organization Name and Address NASA Langley Research Center Hampton, VA 23665		11. Contract or Grant No.
		13. Type of Report and Period Covered Technical Memorandum
12. Sponsoring Agency Name and Address National Aeronautics and Space Administration Washington, DC 20546		14. Sponsoring Agency Code

16. Abstract

A 1/20-size, low-speed flutter model of the SCAT-15F complete airplane was tested in the Langley Transonic Dynamics Tunnel on cables to simulate a near free-flying condition. Only the model wing and fuselage were flexible. Flutter boundaries were measured for a nominal configuration and a configuration with wing fins removed at Mach numbers M from 0.76 to 1.2. For both configurations, the transonic dip in the wing flutter dynamic pressure q boundary was relatively small and the minimum flutter q occurred near $M = 0.92$. Removing the wing fins increased the flutter q about 14 percent and changed the flutter mode from symmetric to antisymmetric. Vibration and flutter analyses were made using a finite-element structural representation and subsonic kernel-function aerodynamics. For the nominal configuration, the analysis (using calculated modal data) predicted the experimental flutter q levels within 10 percent but did not predict the correct flutter mode at the higher M. For the configuration without wing fins, the analysis predicted 16 to 36 percent unconservative (higher than experimental) flutter q levels and showed extreme sensitivity to mass representation details that affected wing tip mode shapes. For high subsonic M, empennage aerodynamics had a significant effect on the predicted flutter boundaries of several symmetric modes. A follow-on research program on arrow-wing flutter is suggested.

17. Key Words (Suggested by Author(s)) Flutter Supersonic Transport Arrow-Wing Wind-Tunnel Test	18. Distribution Statement Unclassified - Unlimited Subject Category 05	
19. Security Classif. (of this report) Unclassified	20. Security Classif. (of this page) Unclassified	21. No. of Pages 14 22. Price* A02